Supporting information for:

Water oxidation on a sustainable polymeric proton relay: Role of post-phosphating of oxide sub-layer on PCET

Materials

All Chemicals and materials in this work were used without further purification. Lysine (Merck, 95%), Cobalt (II) chloride ($CoCl_2$. $6H_2O$, Sigma Aldrich 98%), Ammonium heptamolybdate ($(NH_4)_6Mo_7O_{24}$, Sigma Aldrich 98%), disodium hydrogen phosphate ($Na_2H_2PO_4$, Sigma Aldrich, 98%), urea (CH_4N_2O, Sigma-Aldrich, 98%), potassium phosphate tribasic (K_3PO_4, Sigma Aldrich, 99%), hydrochloric acid (HCl, Merck, 37%), KOH (Sigma-Aldrich, 90%), ethanol (C_2H_5OH, Merck, 99%), acetone (C_3H_6O, Merck). Deuterated electrolytes were prepared using D_2O (Sigma-Aldrich, 99.9 atom % D). All solutions were prepared with deionized water.

Electrochemical measurements

The electrochemical measurements were carried out in aqueous KOH (1.0 M) using Ni foam directly as the working electrode without polymeric binder or conductive additives, a platinum rod as the counter electrode, and a silver/silver chloride electrode (Ag/AgCl) as the reference electrode. All the measured potentials were converted to RHE, $E_{RHE} = E_{Ag/AgCl} + 0.059\ pH + 0.198\ V$. To evaluate the OER activities of the as-papered catalyst, the steady state voltammograms were recorded at a scan rate of 1 mV s^{-1}. Chronopotentiometric measurements were carried out with the same experimental setup without IR correction. Electrochemical impedance spectroscopy (EIS) was performed by applying an alternating voltage with an amplitude of 5 mV in frequency ranges of 0.01 Hz-100 kHz.

Synthesis of NF/$CoMoO_4$

The $CoMoO_4$ was synthesized by a simple hydrothermal reaction. Prior to synthesis, the nickel foam (NF) was purified by soaking it in 3 M HCL for 30 minutes to remove all oxide layers from the surface of the NF. It was then ultrasonically rinsed with ethanol, acetone, and deionized water for 30 minutes and dried at 60 °C overnight. According to the previously reported method [1]. Typically, 0.7 g $CoCl_2$-$6H_2O$ and 0.7 g $(NH_4)_6Mo_7O_{24}$ were mixed in 30 mL deionized water with vigorous stirring for 20 minutes. The NF (1×3 cm) was placed upright on the wall of a 50 mL Teflon-coated stainless-steel autoclave. The resulting solution was transferred to the autoclave to immerse the NF and heated at 130 °C for 13 hours. After the autoclave had cooled down to room temperature, the NF coated with the violet product was washed 3 times with deionized water and ethanol and dried overnight at 50 °C.

Synthesis of amorphous NF/CoMoP

Amorphous-CoMoP were synthesized by a hydrothermal technique. First, the reaction solution was prepared from 0.5 g disodium hydrogen phosphate ($Na_2H_2PO_4$) in 30 ml of deionized water with magnetic stirring. The solution contain of the NF/$CoMoO_4$ piece was transferred to the Teflon-lined 50 ml stainless steel autoclave and heated at 140 °C for 6 hours. This step leads to the apparent change of the NF/$CoMoO_4$ morphology.

Electropolymerization of Poly-Lysine

A piece of the substrate (bare-NF or NF/$CoMoO_4$ and NF/CoMoP, 0.5 cm × 0.5 cm) was subjected for the electropolymerization of lysine through consecutive cyclic voltammetry (CV). The continuous CVs in 0.1 M phosphate buffer solution (PBS) containing 2.5 mM of lysine at pH=8. The electropolymerization was done over the potential range of -1 to 2 V vs. Ag/AgCl at the scan rate of 100 mV/s for 15 cycles [2].

Physical Characterization

Characterization test consist of: X-ray powder diffraction (XRD) measurements were carried out using a Bruker AXS D8 ADVANCE X-ray diffractometer equipped with Cu Kα1 radiation between 10 and 70 °C. X-ray photoelectron spectroscopy (XPS) measurements were performed using a PHI model 590 spectrometer with multi probes (Al Kα radiation, λ = 1486.6 eV) for the investigation of the oxidation state and composition of the material. Scanning electron microscopy (SEM, JEOL JSM-7600F) and energy-dispersive X-ray spectroscopy (EDX) were used to seeking of the morphology and elemental distribution of the composite electrocatalysts. ATR-FTIR analysis was performed by DXR Microscope (Thermo Fisher™). Raman spectroscopy was done using ISB Jobin-Yvon Spex HR-320 equipped with a 600 g/mm monochromator (grating) and an SDL laser with pump wavelength of 785 nm and 140 mw output. The morphology of the samples was studied by TESCAN Mira 3 XMU field emission scanning electron microscope (Czech) coupled with energy dispersive spectroscopy (EDS).

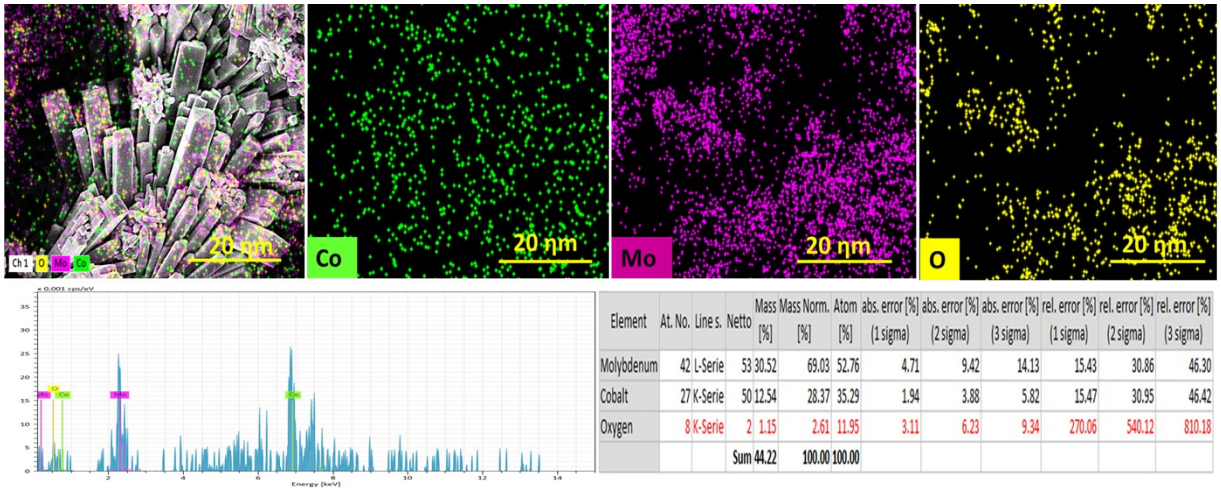

Element	At. No.	Line s.	Netto	Mass [%]	Mass Norm. [%]	Atom [%]	abs. error [%] (1 sigma)	abs. error [%] (2 sigma)	abs. error [%] (3 sigma)	rel. error [%] (1 sigma)	rel. error [%] (2 sigma)	rel. error [%] (3 sigma)
Molybdenum	42	L-Serie	53	30.52	69.03	52.76	4.71	9.42	14.13	15.43	30.86	46.30
Cobalt	27	K-Serie	50	12.54	28.37	35.29	1.94	3.88	5.82	15.47	30.95	46.42
Oxygen	8	K-Serie	2	1.15	2.61	11.95	3.11	6.23	9.34	270.06	540.12	810.18
			Sum	44.22	100.00	100.00						

Figure S1. *The elemental mapping images of the selected area of the NF/$CoMoO_4$ electrode.*

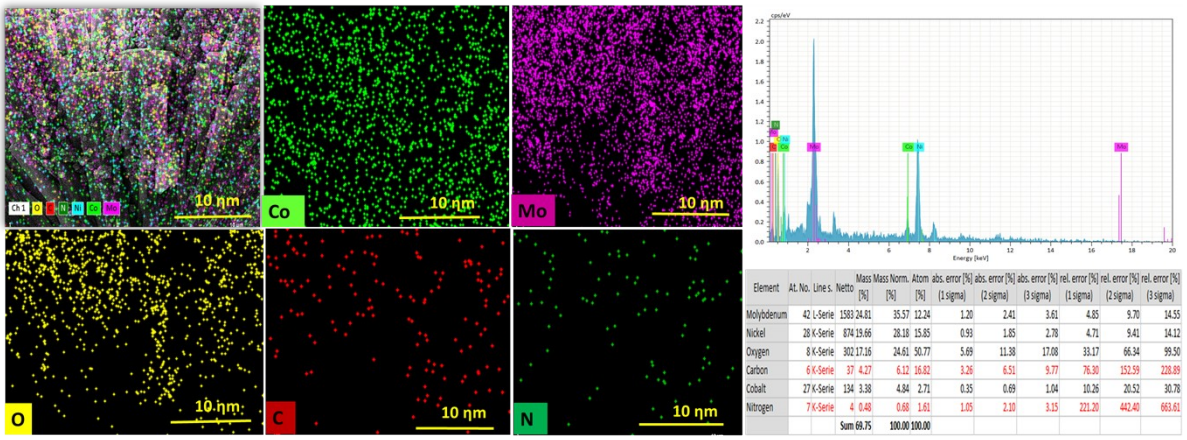

Element	At. No.	Line s.	Netto	Mass [%]	Mass Norm. [%]	Atom [%]	abs. error [%] (1 sigma)	abs. error [%] (2 sigma)	abs. error [%] (3 sigma)	rel. error [%] (1 sigma)	rel. error [%] (2 sigma)	rel. error [%] (3 sigma)
Molybdenum	42	L-Serie	1583	24.81	35.57	12.24	1.20	2.41	3.61	4.85	9.70	14.55
Nickel	28	K-Serie	874	13.66	28.18	15.85	0.93	1.85	2.78	4.71	9.41	14.12
Oxygen	8	K-Serie	302	17.16	24.61	50.77	5.69	11.38	17.08	33.17	66.34	99.50
Carbon	6	K-Serie	37	4.27	6.12	16.82	3.26	6.51	9.77	76.30	152.59	228.89
Cobalt	27	K-Serie	134	3.38	4.84	2.71	0.35	0.69	1.04	10.26	20.52	30.78
Nitrogen	7	K-Serie	4	0.48	0.68	1.61	1.05	2.10	3.15	221.20	442.40	663.61
			Sum	69.75	100.00	100.00						

Figure S2. *The elemental mapping images of the selected area of the NF/CoMoO$_4$/P-lysine electrode.*

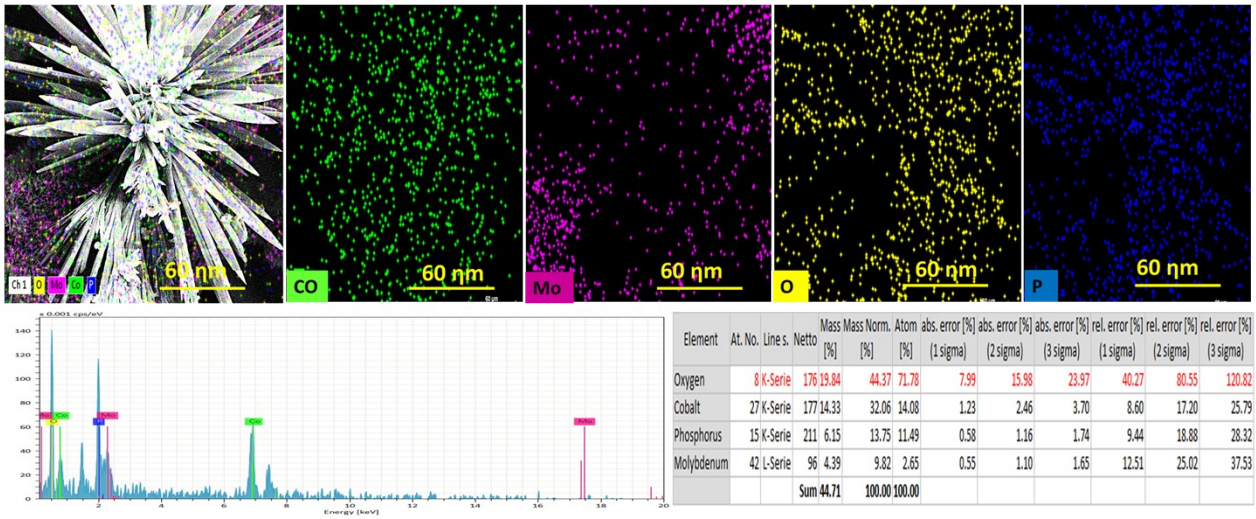

Element	At. No.	Line s.	Netto	Mass [%]	Mass Norm. [%]	Atom [%]	abs. error [%] (1 sigma)	abs. error [%] (2 sigma)	abs. error [%] (3 sigma)	rel. error [%] (1 sigma)	rel. error [%] (2 sigma)	rel. error [%] (3 sigma)
Oxygen	8	K-Serie	176	19.84	44.37	71.78	7.99	15.98	23.97	40.27	80.55	120.82
Cobalt	27	K-Serie	177	14.33	32.06	14.08	1.23	2.46	3.70	8.60	17.20	25.79
Phosphorus	15	K-Serie	211	6.15	13.75	11.49	0.58	1.16	1.74	9.44	18.88	28.32
Molybdenum	42	L-Serie	96	4.39	9.82	2.65	0.55	1.10	1.65	12.51	25.02	37.53
			Sum	44.71	100.00	100.00						

Figure S3. *The elemental mapping images of the selected area of the NF/CoMoP electrode.*

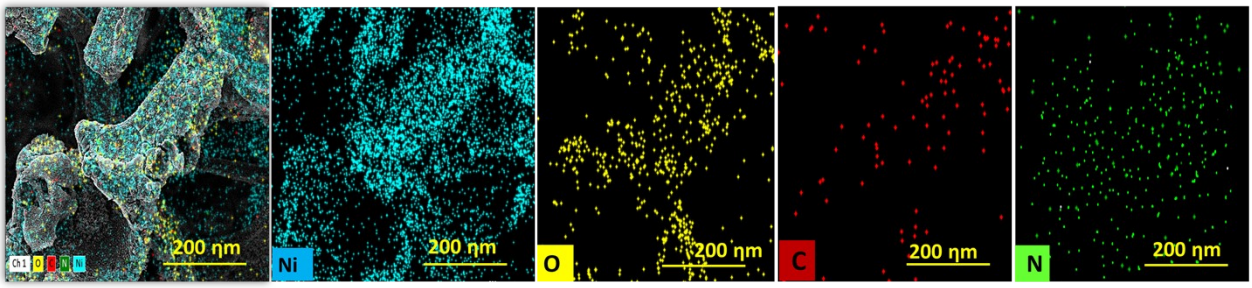

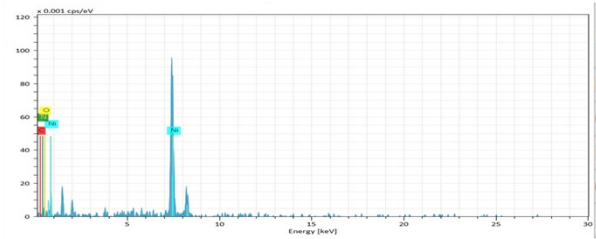

Element	At. No.	Lines.	Netto	Mass [%]	Mass Norm. [%]	Atom [%]	abs. error [%] (1 sigma)	abs. error [%] (2 sigma)	abs. error [%] (3 sigma)	rel. error [%] (1 sigma)	rel. error [%] (2 sigma)	rel. error [%] (3 sigma)
Nickel	28	K-Serie	364	74.71	87.82	63.91	4.56	9.12	13.68	6.11	12.21	18.32
Oxygen	8	K-Serie	5	4.86	5.71	15.26	8.85	17.71	26.56	182.13	364.26	546.39
Nitrogen	7	K-Serie	2	3.63	4.27	13.03	11.21	22.42	33.63	308.36	616.72	925.09
Carbon	6	K-Serie	1	1.87	2.19	7.80	9.09	18.19	27.28	487.55	975.09	1462.64
			Sum	85.07	100.00	100.00						

Figure S4. *The elemental mapping images of the selected area of the NF/P-lysine electrode.*

Element	At. No.	Line s.	Netto	Mass [%]	Mass Norm. [%]	Atom [%]	abs. error [%] (1 sigma)	abs. error [%] (2 sigma)	abs. error [%] (3 sigma)	rel. error [%] (1 sigma)	rel. error [%] (2 sigma)	rel. error [%] (3 sigma)
Oxygen	8	K-Serie	24	16.32	29.37	51.55	14.88	29.76	44.65	91.17	182.35	273.52
Molybdenum	42	L-Serie	95	16.08	28.93	8.47	1.96	3.91	5.87	12.17	24.34	36.50
Cobalt	27	K-Serie	24	8.37	15.05	7.17	1.81	3.62	5.44	21.67	43.33	65.00
Nickel	28	K-Serie	35	7.90	14.21	6.80	1.41	2.83	4.24	17.91	35.81	53.72
Carbon	6	K-Serie	3	4.07	7.32	17.11	9.55	19.09	28.64	234.76	469.52	704.28
Nitrogen	7	K-Serie	2	2.15	3.86	7.74	7.19	14.38	21.57	335.24	670.48	1005.72
Phosphorus	15	K-Serie	7	0.71	1.28	1.16	0.30	0.60	0.90	42.47	84.95	127.42
			Sum	55.59	100.00	100.00						

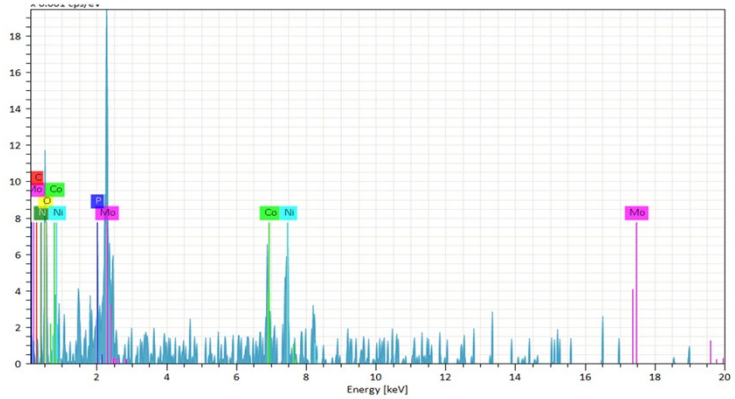

Figure S5. *The elemental mapping images of the selected area of the NF/CoMoP/P-lysine electrode.*

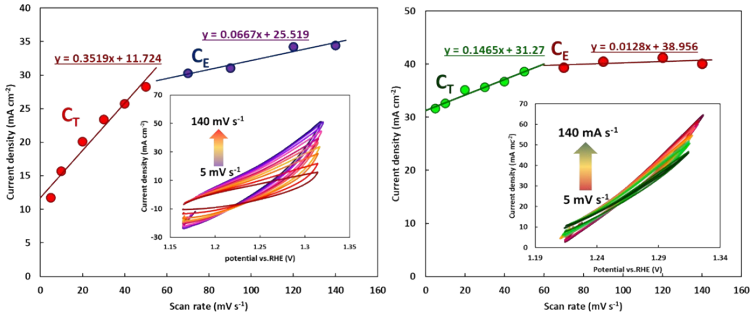

Figure S6. *The CVs obtained in 0.1 M of KOH and the relevant plot of current densities against sweeping rates ranging from 5 to 140 mV* s^{-1} *at (Left) NF/CoMoP and (Right) NF/CoMoP/p-Lys.*

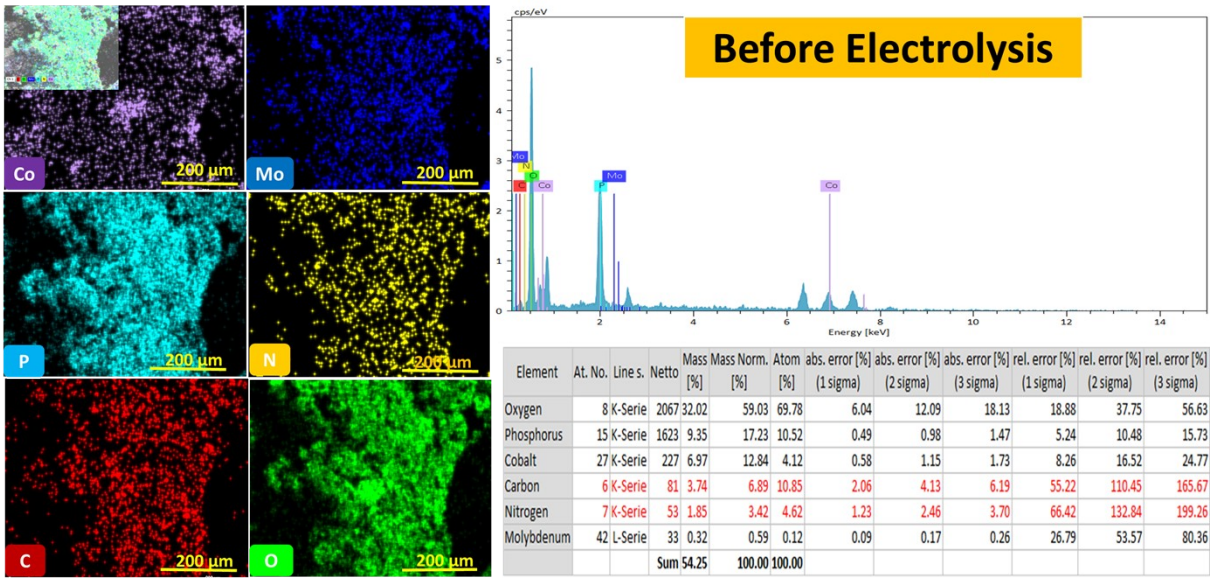

Element	At. No.	Line s.	Netto	Mass [%]	Mass Norm. [%]	Atom [%]	abs. error [%] (1 sigma)	abs. error [%] (2 sigma)	abs. error [%] (3 sigma)	rel. error [%] (1 sigma)	rel. error [%] (2 sigma)	rel. error [%] (3 sigma)
Oxygen	8	K-Serie	2067	32.02	59.03	69.78	6.04	12.09	18.13	18.88	37.75	56.63
Phosphorus	15	K-Serie	1623	9.35	17.23	10.52	0.49	0.98	1.47	5.24	10.48	15.73
Cobalt	27	K-Serie	227	6.97	12.84	4.12	0.58	1.15	1.73	8.26	16.52	24.77
Carbon	6	K-Serie	81	3.74	6.89	10.85	2.06	4.13	6.19	55.22	110.45	165.67
Nitrogen	7	K-Serie	53	1.85	3.42	4.62	1.23	2.46	3.70	66.42	132.84	199.26
Molybdenum	42	L-Serie	33	0.32	0.59	0.12	0.09	0.17	0.26	26.79	53.57	80.36
			Sum	54.25	100.00	100.00						

Figure S7. *The elemental mapping images of the selected area of a typical NF/CoMoP/p-Lys electrode before electrolysis in 0.1 M KOH.*

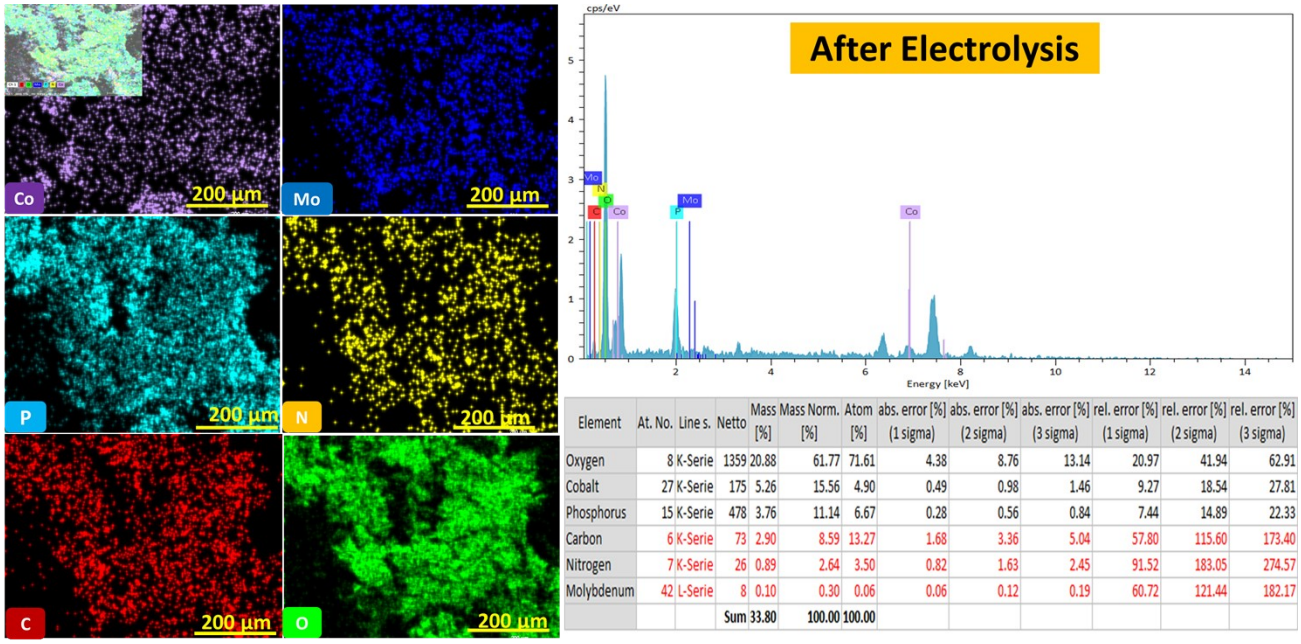

Element	At. No.	Line s.	Netto	Mass [%]	Mass Norm. [%]	Atom [%]	abs. error [%] (1 sigma)	abs. error [%] (2 sigma)	abs. error [%] (3 sigma)	rel. error [%] (1 sigma)	rel. error [%] (2 sigma)	rel. error [%] (3 sigma)
Oxygen	8	K-Serie	1359	20.88	61.77	71.61	4.38	8.76	13.14	20.97	41.94	62.91
Cobalt	27	K-Serie	175	5.26	15.56	4.90	0.49	0.98	1.46	9.27	18.54	27.81
Phosphorus	15	K-Serie	478	3.76	11.14	6.67	0.28	0.56	0.84	7.44	14.89	22.33
Carbon	6	K-Serie	73	2.90	8.59	13.27	1.68	3.36	5.04	57.80	115.60	173.40
Nitrogen	7	K-Serie	26	0.89	2.64	3.50	0.82	1.63	2.45	91.52	183.05	274.57
Molybdenum	42	L-Serie	8	0.10	0.30	0.06	0.06	0.12	0.19	60.72	121.44	182.17
			Sum	33.80	100.00	100.00						

Figure S8. *The elemental mapping images of the selected area of a typical NF/CoMoP/p-Lys electrode employed in electrolysis in 0.1 M KOH for 2 h.*

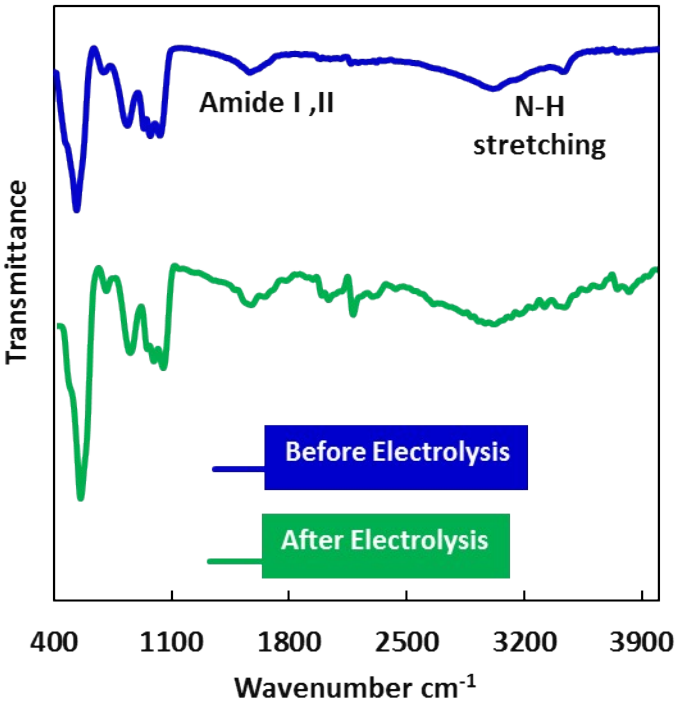

Figure S9. *Comparison of ATR spectra of a typical NF/CoMoP/p-Lys electrode before and after use in electrolysis in 0.1 M KOH for 2 h.*

Supporting Notes:

Supporting Note 1. Kinetic Isotope Effects

KIEs were studied via electrochemical methods. The LSVs were recorded with a scan rate of 5 mV s^{-1} the experiments were carried out in pH adjusted aqueous KOH solution and K_3PO_4 in D_2O solution, the corresponding current densities at a certain overpotential of η were abbreviated as J(H_2O) and J(D_2O). The current density can be expressed by J=nFkC*, where n = total number of electrons transferred, k = heterogeneous rate constant, and C_* = bulk concentration[3].

Dividing J in proteo solution to J in dutero solution gives:

$$\frac{J_{H2O}}{J_{D2O}} = \frac{n_H k_H C_H^*}{n_D k_D C_D^*} \qquad \text{eqn. S1}$$

Since the measurements were performed in solutions with the equal pH (D), the concentration of hydroxide and deuteroxide are same, C^*H=C*D and by assuming unify n values in both solutions, KIE could be written as:

$$KIEs_{,\frac{H}{D}} = \left[\frac{k_{H2O}}{k_{D2o}}\right]_\eta = \left[\frac{J_{H2O}}{J_{D2O}}\right]_\eta \qquad \text{eqn. S2}$$

When measuring pH with the glass electrode in deuterated solution, we often add a constant value of 0.41, PD = pH+0.41. This correction was done via the calculation of electrochemical potential difference between an H_2|Pt electrode in H_2O and a D2|Pt electrode in D_2O [4] . Because no OER dependency observed on [K_3PO_4], it was used as a proton-less basic agent in D_2O solution.

Supporting Note 2. Proton inventory studies

The fitting of the experimental proton inventory data and calculations of the respective parameters (Z and φ) were done through the Equation (1) in the main text, which was derived from the Kresge-Gross-Butler (Eqn. S3)[5]. This equation has been established to describe isotope effect arise from the combination of the isotope effect at a few sites, with the φ values quite different from one, and from a *Z*-effect, an aggregate isotope effect originated from most of sites with φ values individually close to unity [6]:

$$K_n = K_0 \left[\frac{\prod_{i=1}^{x} (1 - n + n\phi Ti)}{\prod_{i=1}^{x} (1 - n + n\phi Ri)} \right] Z^n \qquad \text{eqn.S3}$$

Where k_0 is the kinetic rate constant in deutero solution, kn is the kinetic rate constant in proteo solution. n is the mole fraction of D_2O, x is the number of hydrogenic sites in the reactant/transition state, φ_{Ti} and φ_{Ri} are the isotopic fractionation factor for hydrogenic site in the transition- and reactant-state, respectively. Zn describe the Z-effect, for Z = 1, there are no Z-sites contribution in the isotope effect; for Z > 1, the Z-sites deliver an inverse isotope effect, and for Z < 1, the Z-sites contribute a normal isotope effect [7-9].If we assume a single hydrogenic site, the eqn. S3 could be simplified as :

$$K_n = K_0 \left[\frac{(1 - n + n\varphi T)}{(1 - n + n\varphi R)} \right] Z^n \qquad \text{eqn. S4}$$

We assumed the pronounced kinetics isotope effect occurs at a single hydrogenic site; thus, the x was equal to 1. Assuming J≈k, a simplified form of eqn. S4 is:

$$\frac{j_n}{j_0} = (1 - n + n\,\varphi_{Ti})\, Zn \qquad \text{eqn. S5}$$

Equation S5 was used to fit the proton inventory data, which showed a non-linear dome-shaped curve observed in the case of combination of normal and inverse contributions. A linear curve conveys a single site, a quadratic curve two sites, a cubic curve three sites, and finally an exponential curve indicate an infinite-site model [5, 10, 11]. There are two types of fractionation factors conveyed for hydrogen-transfer reactions on small molecules that involve a *transition state hydrogen bridge*. These two-category pass through a transition-state hydrogen bridges; (I) when the transfer of proton happens through RDS, the labeled hydrogen has an important effect in the reaction-coordinate motion, herein, KIE about 2 to 10 are expected. (II) Another case is when PT is accompanied with another reaction, ET and/or heavy-atom reorganization (such a bond formation between heavier elements than hydrogen)[7, 9].

Supporting Note 3. PH-dependency on RHE scale and atom proton transfer studies

The LSV for pH studies were recorded with a scan rate of 5 mV s^{-1} at different pH values adjusted by KOH solution. All potentials of the measured data were converted into the RHE scale. To convert the standard hydrogen electrode (SHE) scale to the RHE scale, we used the relation $\varepsilon_{RHE} = \varepsilon_{SHE} + 59\ mV \times pH$.[12-27].

The reaction order of the concentration for OH^- is expressed by eqn. S6, where *j* is the current density (mA) at a certain overpotential of η, $[OH^-]$ is the concentration of hydroxide in electrolytes (mol L^{-1}).

$$\rho_{[OH^-]} = \left[\frac{\partial \log J}{\partial \log [OH^-]}\right]_\eta \qquad \text{eqn.S6}$$

Based on the dissociation equilibrium of water, pH+pOH=14, the reaction order of $[OH^-]$ can be described as function of pH, as is in eqn. S7:

$$\rho_{[OH^-]} = \left[\frac{\partial \log J}{\partial \log [-14 + pH]}\right]_\eta = \left[\frac{\partial \log J}{\partial\, pH}\right]_\eta \qquad \text{eqn.S7}$$

In order to designate the involvement of PT in RDS of the catalytic reaction, the dependence of OER activity on an additional Lewis base, PO_4^{-3} , The reaction order of PO_4^{-3}($\rho[PO_4^{-3}]$) was estimated according to eqn. S8:

$$\rho_{[PO_4^{-3}]} = \left[\frac{\partial \log j}{\partial \log [PO_4^{-3}]}\right]_\eta \qquad \text{eqn.S8}$$

Supporting Note 2:

Considering distinct morphological difference between stacked NF/La-PrCH and Fern leaf -shaped structure NF/Sr-La-PrCH, an electrochemical study was established to gain a comparative morphological insight. Figure 3 shows capacitive current graphed obtained at c) NF/La-PrCH and d) NF/Sr-La-PrCH investigated. All graphs clearly show two linear segments, located, respectively, in the low and high sweep rate domains. Inspired by the electrochemical porosity concept [14-15], Da Silva et al. [16] defined the morphology factor (ϕ) as an accumulative parameter to explain the participation of the inner surface of the heterogeneous interfaces to the electrochemical signal:

$$\phi = \frac{C_{d,i}}{C_d} \qquad \text{Eqn. 1}$$

Where, Cd is the differential capacitance consisting of two internal (Cd,i) and external (Cd,e) region of the heterogeneous films, which defines the portion of external and internal surfaces on the overall Cd, which is defined as:

$$C_d = \left(\frac{di_c}{d_v}\right)_E \qquad \text{Eqn. 2}$$

At low scan rate region (5-30 mV s^{-1}), the first linear part in Figure 3 c and d:

$$i_c = C_d \nu \qquad \text{Eqn. 3}$$

Similarly, the second linear part (high can rate domain):

$$i_c = i_{c,r} + C_d \nu \qquad \text{Eqn. 4}$$

Here, ic,r denotes the capacitive current for $\nu \rightarrow 0$

Indeed, the overall capacitive current (ic) is the sum of the capacitive current flowing at the interface of the internal (ic,i), and external (ic,e) regions of the films:

$$i_c = i_{c,i} + i_{c,e} \qquad \text{Eqn. 5}$$

Substitution of Eqs. (3) And (4) in Eq. (5) give Eq. (6):

$$i_{c,i} = C_d \nu - (i_{c,r} + C_{d,e} \nu)$$ Eqn. 6

Finally, differentiation of Eq. (6) vs. ν leads to Eq. (7), allowing the calculation of Cd,i:

$$C_{d,i} = C_d - C_{d,e}$$ Eqn. 7

Cd,i, can be calculated by subtracting the slopes two linear parts (low and high can rates). Finally, the ϕ can be obtained to compare the ratio of Cd,i to Cd. More information is in references 28 and 29.

References

1. D. Guo, H. Zhang, X. Yu, M. Zhang, P. Zhang, Q. Li and T. Wang, *Journal of Materials Chemistry A*, 2013, **1**, 7247-7254.
2. M. Shamsipur, M. Ardeshiri, A. A. Taherpour and A. Pashabadi, *Journal of Materials Chemistry A*, 2021, **9**, 2937-2947.
3. S. Majeed, S. T. R. Naqvi, M. N. ul Haq and M. N. Ashiq, in *Analytical Techniques in Biosciences*, Elsevier, 2022, pp. 157-178.
4. K. A. Rubinson, *Analytical Methods*, 2017, **9**, 2744-2750.
5. A. Kohen and H.-H. Limbach, *Isotope effects in chemistry and biology*, cRc Press, 2005.
6. P. F. Cook and W. Cleland, *Biochemistry*, 1981, **20**, 1805-1816.
7. L. Cao, Q. Luo, J. Chen, L. Wang, Y. Lin, H. Wang, X. Liu, X. Shen, W. Zhang and W. Liu, *Nature Communications*, 2019, **10**, 4849.
8. R. L. Schowen, *Journal of Labelled Compounds and Radiopharmaceuticals: The Official Journal of the International Isotope Society*, 2007, **50**, 1052-1062.
9. K. Venkatasubban and R. L. Schowen, *Critical Reviews in Biochemistry*, 1984, **17**, 1-44.
10. P. F. Fitzpatrick, *Biochimica et Biophysica Acta (BBA)-Proteins and Proteomics*, 2015, **1854**, 1746-1755.
11. M. Tao, J. Bacsa and Y. Geletii, *Studies of Electronically Perturbed Polyoxometalate Catalysts*, 25.
12. L. Zhong, J. Ding, X. Wang, L. Chai, T.-T. Li, K. Su, Y. Hu, J. Qian and S. Huang, *Inorganic Chemistry*, 2020, **59**, 2701-2710.
13. U. P. Suryawanshi, M. P. Suryawanshi, U. V. Ghorpade, M. He, D. Lee, S. W. Shin and J. H. Kim, *ACS Applied Energy Materials*, 2020, **3**, 4338-4347.
14. F. Yang, X. Chen, Z. Li, D. Wang, L. Liu and J. Ye, *ACS Applied Energy Materials*, 2020, **3**, 3577-3585.
15. S. Bera, W.-J. Lee, E.-K. Koh, C.-M. Kim, S. Ghosh, Y. Yang and S.-H. Kwon, *The Journal of Physical Chemistry C*, 2020, **124**, 16879-16887.
16. M. Cai, W. Liu, X. Luo, C. Chen, R. Pan, H. Zhang and M. Zhong, *ACS applied materials & interfaces*, 2020, **12**, 13971-13981.
17. H. R. Devi, R. Nandan and K. K. Nanda, *ACS applied materials & interfaces*, 2020, **12**, 13888-13895.
18. N.-U.-A. Babar and K. S. Joya, *ACS omega*, 2020, **5**, 10651-10662.
19. X. Bu, C. Chiang, R. Wei, Z. Li, Y. Meng, C. Peng, Y. Lin, Y. Li, Y. Lin and K. S. Chan, *ACS applied materials & interfaces*, 2019, **11**, 38633-38640.
20. M. A. Ehsan, A. S. Hakeem, M. Sharif and A. Rehman, *ACS omega*, 2019, **4**, 12671-12679.
21. S. Hao, G. Zheng, S. Gao, L. Qiu, N. Xu, Y. He, L. Lei and X. Zhang, *ACS Sustainable Chemistry & Engineering*, 2019, **7**, 14361-14367.
22. J.-T. Ren and Z.-Y. Yuan, *ACS Sustainable Chemistry & Engineering*, 2017, **5**, 7203-7210.

23. M. P. Suryawanshi, U. V. Ghorpade, S. W. Shin, U. P. Suryawanshi, E. Jo and J. H. Kim, *ACS Catalysis*, 2019, **9**, 5025-5034.
24. B. Owens-Baird, J. P. Sousa, Y. Ziouani, D. Y. Petrovykh, N. A. Zarkevich, D. D. Johnson, Y. V. Kolen'ko and K. Kovnir, *Chemical science*, 2020, **11**, 5007-5016.
25. M. Yao, B. Sun, L. He, N. Wang, W. Hu and S. Komarneni, *ACS Sustainable Chemistry & Engineering*, 2019, **7**, 5430-5439.
26. Q. Zhang, S. Zhang, Y. Tian and S. Zhan, *ACS Sustainable Chemistry & Engineering*, 2018, **6**, 15411-15418.
27. Q. Zhang, N. Liu and J. Guan, *ACS Applied Energy Materials*, 2019, **2**, 8903-8911.
28. A. J. Bard. L. R. Faulkner, Fundamentals and applications. Electrochemical methods 2001, 2 (482), 580-632.
29. K. A. Rubinson, Practical corrections for p (H, D) measurements in mixed H2O/D2O biological buffers. Analytical Methods 2017, 9 (18), 2744-2750.